



Catalytically impaired TrpA subunit of tryptophan synthase from *Chlamydia trachomatis* is an allosteric regulator of TrpB

Karolina Michalska^{1,2} | Samantha Wellington³ | Natalia Maltseva¹ | Robert Jedrzejczak¹ | Nelly Selem-Mojica⁴ | L. Rodrigo Rosas-Becerra⁴ | Francisco Barona-Gómez⁴  | Deborah T. Hung³ | Andrzej Joachimiak^{1,2,5} 

¹Center for Structural Genomics of Infectious Diseases, University of Chicago, Chicago, Illinois

²Structural Biology Center, X-ray Science Division, Argonne National Laboratory, Argonne, Illinois

³Department of Genetics, Broad Institute of MIT and Harvard, Cambridge, Massachusetts

⁴Evolution of Metabolic Diversity Laboratory, Unidad de Genómica Avanzada (Langebio), Cinvestav, Mexico

⁵Department of Biochemistry and Molecular Biology, University of Chicago, Chicago, Illinois

Correspondence

Andrzej Joachimiak, X-ray Science Division, Argonne National Laboratory, 9700 South Cass Avenue, Building 446, Argonne, IL 60439, USA.
Email: andrzejj@anl.gov

Funding information

National Institute of Allergy and Infectious Diseases, Grant/Award Numbers: HHSN272201200026C, HHSN272201700060C; Newton Advanced Fellowship of the Royal Society, Grant/Award Numbers: CB-2016-01 285746, NAF\R2\180631; Office of Science, Grant/Award Number: DE-AC02-06CH11357

Abstract

Intracellular growth and pathogenesis of *Chlamydia* species is controlled by the availability of tryptophan, yet the complete biosynthetic pathway for L-Trp is absent among members of the genus. Some representatives, however, preserve genes encoding tryptophan synthase, TrpAB – a bifunctional enzyme catalyzing the last two steps in L-Trp synthesis. TrpA (subunit α) converts indole-3-glycerol phosphate into indole and glyceraldehyde-3-phosphate (α reaction). The former compound is subsequently used by TrpB (subunit β) to produce L-Trp in the presence of L-Ser and a pyridoxal 5'-phosphate cofactor (β reaction). Previous studies have indicated that in *Chlamydia*, TrpA has lost its catalytic activity yet remains associated with TrpB to support the β reaction. Here, we provide detailed analysis of the TrpAB from *C. trachomatis* D/UW-3/CX, confirming that accumulation of mutations in the active site of TrpA renders it enzymatically inactive, despite the conservation of the catalytic residues. We also show that TrpA remains a functional component of the TrpAB complex, increasing the activity of TrpB by four-fold. The side chain of non-conserved β Arg267 functions as cation effector, potentially rendering the enzyme less susceptible to the solvent ion composition. The observed structural and functional

The submitted manuscript has been created by UChicago Argonne, LLC, Operator of Argonne National Laboratory (“Argonne”). Argonne, a U.S. Department of Energy Office of Science laboratory, is operated under Contract No. DE-AC02-06CH11357. The U.S. Government retains for itself, and others acting on its behalf, a paid-up nonexclusive, irrevocable worldwide license in said article to reproduce, prepare derivative works, distribute copies to the public, and perform publicly and display publicly, by or on behalf of the Government.

This is an open access article under the terms of the Creative Commons Attribution-NonCommercial-NoDerivs License, which permits use and distribution in any medium, provided the original work is properly cited, the use is non-commercial and no modifications or adaptations are made.

© 2021 The Authors. *Protein Science* published by Wiley Periodicals LLC on behalf of The Protein Society.

changes detected herein were placed in a broader evolutionary and genomic context, allowing identification of these mutations in relation to their *trp* gene contexts in which they occur. Moreover, in agreement with the *in vitro* data, partial relaxation of purifying selection for TrpA, but not for TrpB, was detected, reinforcing a partial loss of TrpA functions during the course of evolution.

KEYWORDS

allosteric regulation, biosynthesis, catalysis, crystal structure, tryptophan

1 | INTRODUCTION

Chlamydia trachomatis is the etiological agent of chlamydia – one of the most common sexually transmitted diseases in the United States. According to the Centers for Disease Control and Prevention (CDC), 1,758,668 chlamydial infections were reported in 2018 (~ 3 million total), showing a steadily increasing rate since 2013. Worldwide, the WHO estimated that in 2012, 131 million people were infected with a number of *Chlamydia* species.¹ Different biovars of *C. trachomatis*, each of which can be further divided into serovars or genotypes, cause genital (serovars D-K), ocular (trachoma; serovars A, B, Ba, C) or lymphoid tissue (lymphogranuloma venereum, L1, L2, L3) infections. The genital variant of the disease, often asymptomatic, can lead to serious health problems when untreated, especially for women. The potential complications include pelvic inflammatory disease, ectopic pregnancy, endometritis, salpingitis, tubal factor infertility, and epididymitis in males. The infection can be passed during birth onto the infants who may develop conjunctivitis and/or pneumonia. Common treatment is a combination of two antibiotics, azithromycin (macrolide family) and doxycycline (tetracycline family), with alternative options available for pregnant women and infants. Those therapies are considered safe and effective, although a high rate of recurrence is observed, due to reinfection and bacterial persistence. Moreover, *C. trachomatis* shows early signs of antibiotic resistance,^{2–4} adding more concern to the increase of sexually transmitted diseases and shrinking treatment options. More troubling is that trachoma-causing serovars are easily transmitted through personal contact (via hands, clothes or bedding) and by flies that touch infected surfaces. It is the leading infectious cause of irreversible blindness, classified as a neglected tropical disease, affecting primarily developing countries with 158 million people potentially impacted. New drug targets and treatments are urgently needed.

Besides *C. trachomatis*, the genus *Chlamydia* contains several other members, which despite common biology,

display broad host tropism. *C. pneumoniae* is another human pathogen responsible for atypical pneumonia⁵ and chronic inflammatory diseases.⁶ It can also infect a variety of animals.⁷ Other animal infecting species include *C. muridarum* (mice and hamsters), *C. suis* (pig and wild boar), *C. pecorum* (ruminants, koala), *C. abortus* (ruminants), *C. caviae* (guinea pig), and *C. felis* (cats). One interesting exception is *C. psittaci* infecting birds and causing bird-borne disease psittacosis in humans.⁸

The organisms referenced above are obligate intracellular pathogens. Their growth leads through a biphasic developmental cycle, lasting 48–72 hr (reviewed by Abdelrahman et al.).⁹ The host is infected by a non-replicative extracellular form termed elementary body (EB), which upon attachment to epithelial cell becomes internalized into membrane-bound vacuoles, known as inclusions. Subsequently, most EBs differentiate into reticulate bodies (RB), representing a metabolically active form of the bacterium. RBs then replicate inside the growing inclusions and later undergo another differentiation event back to EBs. Eventually, host cell lysis leads to the release of EBs to the extracellular environments where they are ready to infect neighboring cells. Under stress conditions, such as nutrient starvation, antibiotics or immunological response, the developmental cycle is disrupted: chlamydial cells do not divide or produce infectious particles. However, they still multiply their chromosomes, resulting in aberrant, enlarged RBs (aRBs) and other morphological changes, and bacteria enter a viable but non-cultivable persistent state (reviewed by Hogan et al.).¹⁰ aRBs can survive unfavorable environments for a prolonged time. Once the stress factor is removed, they can resume normal growth.

One of the best-understood stimuli of chlamydial persistence in humans is gamma interferon, IFN γ . This cytokine plays a major role in innate and adaptive immunity regulating host defense mechanisms against infectious agents. IFN γ upregulates expression of indoleamine 2,3-dioxygenase (IDO) – one of the enzymes from the kynurenine pathway of tryptophan catabolism. IDO

converts L-Trp to *N*-formylkynurenine, effectively eliminating L-Trp in all cell types where the enzyme is present. Bacterial survival, however, depends on access to amino acids, including L-Trp, which could be imported or synthesized *de novo*. The entire pathway for L-Trp biosynthesis, starting from the chorismate precursor, requires seven enzymes (TrpA–TrpG) and 78 ATP molecules.¹¹ Given such a high metabolic burden, the synthetic route is highly regulated on multiple levels and is only utilized when necessary. In several pathogens, for example in *M. tuberculosis*^{12,13} and *Francisella tularensis*,¹⁴ IFN γ -induced IDO activity turns on bacterial L-Trp production. *Chlamydia*, however, due to their obligate intracellular lifestyle and seemingly plentiful host resources, contain significantly reduced genomes ranging from 1 to 1.5 Mbp, with limited metabolic capabilities. Among several amino acid auxotrophies, they have lost some or all genes needed for L-Trp biosynthesis. For example, *C. pneumoniae* is missing all the L-Trp pathway enzymes, *C. psittaci* GPIC lacks anthranilate synthase, necessary for the two first steps of biosynthesis, while *C. trachomatis* maintains only tryptophan synthase (TrpAB), catalyzing the final two reactions of L-Trp biosynthesis.

Tryptophan synthase is a bifunctional protein–protein complex consisting of two subunits: α , encoded by *trpA*, and β , encoded by *trpB*. The enzyme operates as an $\alpha\beta\alpha$ heterotetramer. Several orthologous enzymes have been characterized so far, including complexes from *Salmonella typhimurium* (*St*),^{15–30} *Mycobacterium tuberculosis* (*Mt*),¹³ *Streptococcus pneumoniae* (*Sp*), *F. tularensis* (*Ft*),³¹ *Pyrococcus fusarium* (*Pf*)^{32,33} and *Sulfolobus solfataricus* (*Ss*), as well as TrpA components from *Legionella pneumophila* (*Lp*),³¹ and *Escherichia coli* (*Ec*).^{34,35} The *S. typhimurium* enzyme has been most extensively studied, providing information about catalysis, mutants, cation effects, ligand binding, regulation, and conformational rearrangements linked to reaction stages.

Structurally, TrpA is a TIM-barrel, whereas TrpB consists of two 3-layer ($\alpha\beta\alpha$) sandwich domains. TrpA converts indole-3-glycerol phosphate (IGP) into glyceraldehyde-3-phosphate (G3P) and indole (IND), and TrpB, in a reaction dependent on pyridoxal 5'-phosphate (PLP), catalyzes the β -replacement reaction in which indole displaces the hydroxyl group of L-Ser to produce L-Trp. While the two $\alpha\beta$ halves of the complex act independently, the activities of α and β units within each $\alpha\beta$ heterodimer are highly coordinated. The network of allosteric interactions and orchestrated structural rearrangements, involving loop α L6 of TrpA and the communication domain (COMM) of TrpB,¹⁸ increases activity of TrpA in the presence of indole-ready intermediate in TrpB and *vice versa* – indole production in TrpA activates TrpB in L-Ser conversion.³⁶ Therefore, both subunits carry out two functions: catalysis and allosteric regulation.

Prior analysis of *C. trachomatis* genomic data showed high heterogeneity within *trpA* and *trpB* genes—ocular variants contain deletions and frameshift mutations, none of which have been found in genital strains. Most changes are found in *trpA* homologs, which share some features of the functional enzyme, for example, they maintain catalytic residues, however, they carry multiple mutations in their vicinity. Substitutions have been also found in loop α L6 of TrpA, which is critical in allosteric communication between subunits, raising doubts about the enzyme functionality. Indeed, no activity was observed for α reaction in genetic complementation studies or with cell lysates expressing *CtTrpA* and *CtTrpB*.³⁷ TrpB, on the other hand, is much more conserved. In addition, previous studies showed that *CtTrpB* is a functional enzyme carrying out β reaction, though strongly dependent on the presence of *CtTrpA*, even if catalytically incompetent. Based on these observations, it was proposed that genital *C. trachomatis* serovars are able to escape L-Trp starvation via TrpB catalyzed conversion of indole to L-Trp, with the substrate provided by co-inhabiting bacteria. Indole is a common signaling molecule produced by a variety of prokaryotic species and could thus be available for *C. trachomatis*. Ocular strains, occupying a much more sterile niche, do not have indole in the environment and apparently lost capability to utilize it.³⁸

Here, we sought to provide a detailed analysis of *C. trachomatis* D/UW-3/CX tryptophan synthase (*CtTrpAB*). We have used structural and biochemical data combined with updated comparative genomic analysis to study the enzyme properties. Our results corroborate previous reports that the β subunit is fully functional and is using indole as a substrate to produce L-Trp. The structural model enables us to interpret the α subunit mutations in the three dimensional context to explain *CtTrpA* inability to produce indole from IGP. While catalytically incompetent, *CtTrpA* still exerts an allosteric effect on the *CtTrpB* catalytic properties, increasing its activity almost four times, thus providing metabolic advantage. In agreement with these results, *CtTrpA* was found to be under relaxation of purifying selection, whereas *CtTrpB* showed signs of intensifying selection. The two hundred fifty plus genomes analyzed provide an evolutionary context in which the identified mutations take place, which coincide with serovars specificity and ecological niche.

2 | RESULTS AND DISCUSSION

2.1 | Enzymatic properties

Previous genetic analysis, *in vivo* studies and limited *in vitro* assays, have shown that TrpAB from genital strains of *C. trachomatis* retains the ability to make L-Trp

from indole but not from glyceraldehyde-3-phosphate.^{37,38} Interestingly, TrpA, though unable to carry out the α reaction, was shown to be necessary for the TrpB-catalyzed transformation. We have expressed and purified recombinant TrpAB $\alpha\beta\beta\alpha$ complex from *C. trachomatis* D/UW-3/CX to investigate in detail their catalytic and structural properties.

We measured the activity of the *Ct*TrpAB complex and of each of the subunits individually in both the α reaction using IGP as a substrate, and in the β reaction using indole and L-Ser as substrates. Both *Ct*TrpB and the *Ct*TrpAB complex were active in the β -elimination reaction. Similarly to other TrpAB homologs^{39–41} (Table 1), the *Ct*TrpAB complex was more active than *Ct*TrpB alone ($k_{\text{cat}}^{\beta} = 21.1 \pm 3.7 \text{ min}^{-1}$ and $5.9 \pm 1.8 \text{ min}^{-1}$ for *Ct*TrpAB and *Ct*TrpB, respectively). The K_{M} for L-Ser was similar for the heterotetrameric complex and *Ct*TrpB alone ($K_{\text{M}}^{\text{Ser}} = 2.1 \pm 1.0 \text{ mM}$ and $1.6 \pm 0.3 \text{ mM}$ for *Ct*TrpAB and *Ct*TrpB, respectively).

In contrast to the β -elimination reaction, neither *Ct*TrpA nor the *Ct*TrpAB complex were proficient at catalyzing the α reaction. For *Ct*TrpA alone, the α reaction was so slow as to be unmeasurable. The *Ct*TrpAB complex was also a very poor catalyst of the α reaction with k_{cat}^{α} of only $0.29 \pm 0.1 \text{ min}^{-1}$. Unlike in other TrpAB homologs,⁴² adding L-Ser did not accelerate the α reaction.

2.2 | Structure of CtTrpAB

To reveal structural basis of the observed differences in enzymatic activity, we have determined the crystal structure of the *Ct*TrpAB complex. As expected, the enzyme preserves the canonical heterotetrameric architecture. The crystal lattice contains a single $\alpha\beta$ module in the asymmetric unit, the other $\alpha'\beta'$ module is related by crystallographic two-fold symmetry. In the absence of physiological ligands, the TrpAB complex has been captured in the double-open $\alpha^{\text{O}}\beta^{\text{eO}}$ state, characterized by the disordered loop αL6 (residues $\alpha\text{Q178}-\alpha\text{E184}$) of TrpA and the TrpB COMM domain pushed away from the second TrpB domain, as well as from TrpA. The β^{eO} denotes expanded open conformation similar to the one observed previously for *Mt*TrpAB.¹³ Besides loop αL6 , unmodeled residues include N-terminal methionine residues in both subunits and the His₆-tag appended at the C-terminus of the TrpB. The two protein chains show high overall similarity to the previously characterized tryptophan synthases with root mean square deviations for C α atoms superpositions ranging from 1.66 to 2.29 Å for TrpA and 0.78–2.07 Å for TrpB (Figure 1). As observed before, sequence and fold conservation is higher for TrpB (~50% sequence identity), which does not show any reorganization in secondary structure elements or loops (Figures 1, 2). On the other hand, TrpA, with only 22–25% sequence identity,

TABLE 1 Kinetic parameters of characterized TrpABs. Unless stated otherwise, the parameters correspond to the reactions measured within the complex

	<i>Sp</i> TrpAB ³¹	<i>Ft</i> TrpAB ³¹	<i>Lp</i> TrpAB ³¹	<i>Mt</i> TrpAB ¹³	<i>St</i> TrpAB ⁶⁰	<i>Ec</i> TrpAB ³⁹	<i>Ct</i> TrpAB (this work)
$k_{\text{cat}}^{\alpha\beta}$				19 min ⁻¹ with IGP	222 min ⁻¹ with IGP		
k_{cat}^{β}	15.0 min ⁻¹ with IND	78.6 min ⁻¹ with IND	1.7 min ⁻¹ with IND	197 min ⁻¹ with IND	324 min ⁻¹ with IND	228 min ⁻¹ with IND 16.2 min ⁻¹ in isolated TrpB	21.1 min ⁻¹ (5.9 min ⁻¹ in isolated TrpB)
k_{cat}^{α}				19.6 min ⁻¹	18 min ⁻¹		0.29 min⁻¹ unmeasurable in isolated TrpA) Ser has no influence
$K_{\text{M}}^{\text{Ser}}$	18.3 mM with IND	25.0 mM with IND	43.2 mM with IND	0.50 mM with IGP 4.4 with IND	0.6 mM with IND		2.1 mM with IND (1.6 mM in isolated TrpB)
$K_{\text{M}}^{\text{IND}}$	9.9 μM with Ser	11.6 μM with Ser	10.8 μM with Ser	32.0 μM with Ser	60 μM with Ser	7.40 μM with Ser 9.4 μM in isolated TrpB	<25 μM
$K_{\text{M}}^{\text{IGP}}$				32.6 μM with Ser	10 μM with Ser		

Abbreviations: IGP, indole-3-glycerol phosphate; IND, indole.

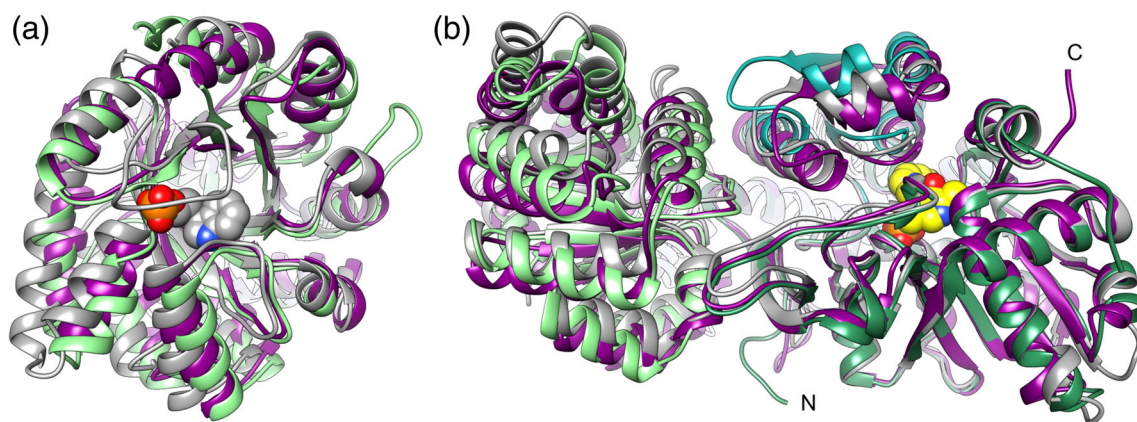


FIGURE 1 Structure comparison with orthologous TrpABs. (a). Superposition of TrpAs extracted from the TrpAB heterodimers: *Ct*TrpA (green), *Mt*TrpA (purple; chain C, Protein Data Bank [PDB] ID 5TCF), *St*TrpA (grey; chain A, PDB ID 1QOP). *St*TrpA indole 3-propanol phosphate ligand is shown in sphere representation. (b). Superposition of TrpBs: *Ct*TrpB (dark green/cyan), *Mt*TrpB (purple; chains D), and *St*TrpB (grey; chain B). Pyridoxal 5'-phosphate (PLP) cofactor from *Ct*TrpAB is shown in a sphere representation, TrpA is shown to indicate mutual orientations of the subunits

displays some features absent in other homologs (Figure 2). The most prominent are the differences in two loops: α L4 is four residues longer than in other TrpAs, while α L6 is shorter by the same number of residues. The consequences of the former insertion are not clear – the fully ordered α L4 loop is relatively far from the TrpA active site, it is solvent-exposed and does not contact with TrpB. In contrast, loop α L6 is in close proximity to the catalytic pocket and has been shown to play an important role in catalysis and allosteric communication. This structural element remains flexible in the absence of TrpA ligands and closes over the active site only when the substrate or inhibitor is bound. In *Ct*TrpA, α L6 remains disordered too, however, here this loop is not only shorter, but also the highly conserved GVTG sequence motif is replaced by ATRD, raising questions about its ability to seal the binding site.

2.3 | *Ct*TrpA active site

The canonical TrpA active site is located on the top of the central β -barrel and preserves two catalytic residues – α Asp55 and α Glu44 (Figure 3). α Asp55 (*St* α Asp60) is contributed by the loop α L2 that faces the TrpB subunit, while α Glu44 (*St* α Glu49) is located on the α S2 element of the protein core. The pocket carries several notable mutations protruding much larger side chains into the catalytic cavity. For example, the α S2 strand contains α Arg205, replacing conserved Gly (*St* α Gly211) and α S8 brings α Lys227 instead of another conserved Gly (*St* α Gly234). These two residues form salt bridges with the key catalytic acids: α Lys227 with α Asp55 and

α Arg205 with α Glu44, practically locking their orientations. In addition, α Ile123 takes the place of slightly smaller Pro, Val and Ala (*St* α Ala129). α Tyr95 from α S3 not only substitutes much more flexible Met or smaller Leu (*St* α Leu100) adding a bulkier residue to the pocket, but also forms a hydrogen bond with catalytic α Asp55. These changes appear to reduce the cavity volume, especially in the indole-binding subpocket. In fact, in superposition with the *S. typhimurium* TrpA structure co-crystallized with indole 3-propanol phosphate (Protein Data Bank [PDB] ID 1QOP²⁰), α Arg205 and α Lys227 clash with the indole ring. In addition, the large side chain of α Arg205 rearranges α Tyr173 to form a hydrogen bond with catalytic α Glu44. In other orthologs, the Tyr equivalent (*St* α Tyr175) is rotated toward the substrate tail binding subpocket.

Besides α Arg205, the α S2 strand carries two other important substitutions – α Asp207, exchanging yet another conserved Gly (*St* α Gly213), and α Arg206, replacing hydrophobic side chains (*St* α Phe212) that in the TrpA closed state stacks against the IGP substrate indole ring. In the current structure of *Ct*TrpA, α Arg206 faces the protein surface, resembling other homologs captured in the open state. While different in physical properties, the arginine residue could functionally replace other side chains' interactions with indole, either via π - π interactions or H- π hydrogen bonds, combined with electrostatic forces of cation- π attractive forces. α Asp207 partly mimics the phosphate group of the substrate molecule interacting with the main-chain amino groups of α Val226 (*St* α Ser233) and α Lys227 (*St* α Gly234) as well as the side chain of α Thr228 (*St* α Ser235). Overall, numerous substitutions

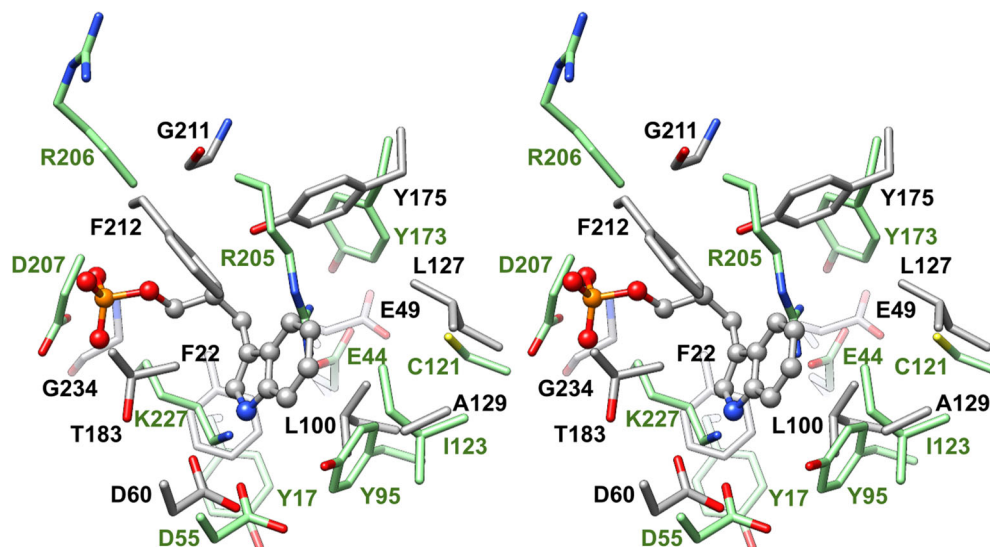


FIGURE 3 TrpA active site. Stereoview of active site superposition of *Ct*TrpA (green) with *St*TrpA (grey, chain A, Protein Data Bank [PDB] ID 1QOP)

subdomains. In comparison with previously characterized enzymes, the β active site is mostly conserved at both sequence and structure level for the PLP cofactor and side chains, with a few exceptions. In agreement with this, it contains two catalytic residues β Thr107 and β Asp302 (in *St*TrpA β Thr110 and β Asp305, respectively). The sulfate ion binds into the substrate serine binding site, interacting with the main-chain amino groups of β Gly108, β Ala109 and β His112. It forms additional hydrogen bonds with the hydroxyl group of β Thr107 and β Tyr303. With the exception of β Ala109 and β Tyr303, these interactions mimic the pattern observed for the carboxylate group of the substrate. The phosphate group of PLP is anchored by interaction with the N-terminal dipole of helix β H9, where it forms direct hydrogen bonds with several main-chain amino groups and three conserved side chains (β His83, β Ser232 and β Asn233). The only notable deviation in the PLP binding site architecture is the unusual conformation of β Gln111 (*St* β Gln114, *Mt* β Gln128, *Sp* β Gln118) from the COMM domain: in the current structure it bridges over to the other subdomain via a weak hydrogen bond with β Glu347.

β Tyr303 is not a conserved residue: in *St*TrpB and *Ft*TrpB it is replaced by Phe (306 and 305, respectively), but it is preserved in *Mt*TrpB (β Tyr320). The aromatic side chain has been shown to interact with the indole ring via T-stacking (PDB ID 5CGQ and^{16,28,29}), where the residue contributes π electrons. Therefore it is somewhat surprising that the Tyr/Phe side chain is not fixed, but adopts generally two different conformations in the compared structures: facing either the PLP moiety and the COMM domain, or the Phe278/Phe279 sequence in the S9a/S9b hairpin and the loop between S6 and H7 at TrpB/TrpA interface. The conformation appears to primarily depend on the latter environment. In the presence

of a smaller side chain in position 189, for example alanine (*St* β Ala192, *Mt* β Ala206) or valine (*Pf* β Val187), Tyr/Phe can fit in its neighborhood. In the current structure and in *Sp*TrpB, the bulkier side chain of β Leu189 directs β Tyr303 toward the TrpB active site. This movement is accompanied by the rearrangement of β Ser305 (*St* β Ser308). In *Mt*TrpAB and *St*TrpAB the rotamer of Tyr/Phe does not change upon ligand binding or conformational state of TrpB. If the same holds true for the *Chlamydia* enzyme, the residue aromatic ring would engage with the indole moiety via π - π interactions rather than T-stacking (Figure 4). One has to note, however, that the current position of the aromatic side chain in *Ct*TrpAB may not be compatible with the closed conformation of TrpB, as β Leu163 would clash with β Tyr303, requiring some rearrangement.

2.5 | Cation binding site

The activity of TrpAB and the equilibrium distribution of its forms is affected by monovalent cations. Large ions, such as NH_4^+ or Cs^+ , stabilize the closed conformation and increase reaction rate five-fold.⁴³ Small cations, K^+ or Na^+ , are also activators, though less potent, and promote the open state. A similar effect is induced by guanidinium at low concentrations.⁴⁴ The cations bind to a dedicated site close to the TrpB active site. The typical coordination sphere consists of main-chain carbonyl groups (β Val231, β Gly232, β Gly268, β Leu304, β Phe306, β Ser308 in *St*TrpB) that are sometimes replaced by water molecules, depending on the ion size.¹⁵ Two side chains face the cation but do not participate in binding: *St* β Asp256 and *St* β Pro270. The latter position is variable among homologs, for example, *Mt*TrpB contains β Thr284 that utilizes the hydroxyl group for metal anchoring.¹³

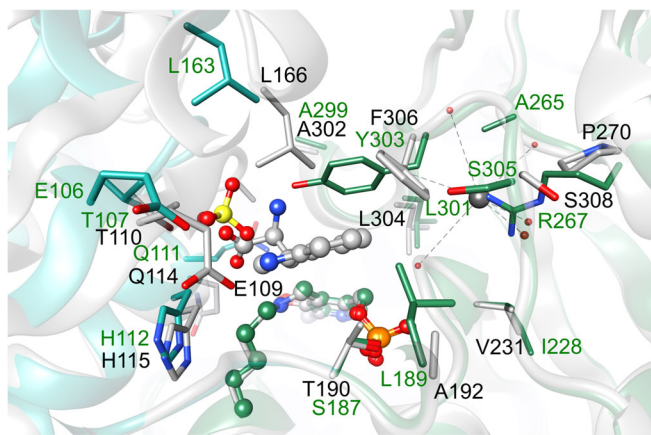


FIGURE 4 TrpB active site. Active site superposition of *Ct*TrpB (green) with *St*TrpB in complex with L-Trp (grey, chain B, Protein Data Bank (PDB) ID 5CGQ). The L-Trp ligand and Lys-pyridoxal 5'-phosphate (PLP) adduct are shown in a ball-and-stick model. Cesium cation from the *St*TrpB structure is shown as a sphere

The overall architecture of the cation binding pocket is preserved in *Ct*TrpB, with β Ile228, β Gly229, β Ala265, β Leu301, β Tyr303, and β Ser305 presenting their main-chain carbonyl groups for cation coordination. However, *St* β Pro270 is replaced by β Arg267, bringing a novel structural feature previously not seen in any TrpB. Namely, the guanidinium group occupies the cation pocket and binds to carbonyl groups of β Tyr303, β Gly229, β Ile228, as well as to the side chain of β Glu253. Such interactions have been proposed previously based on the biochemical and modeling data with guanidine hydrochloride but never experimentally observed.⁴⁴ Since in *Ct*TrpAB the guanidinium group is an element of the protein rather than the solvent component, it appears that β Arg267 plays the role of a permanently present cation (Figure 5). It therefore suggests that the enzyme activity may be independent of the solution composition, at least with respect to the ion binding in the TrpB active site.

2.6 | Comparative evolutionary genomics of TrpAB in *Chlamydia*

Sequences of nearly 300 TrpA and TrpB proteins from *Chlamydia* and closely related organisms were retrieved with BLAST and CORASON.⁴⁵ Multiple sequence alignments and phylogenetic trees constructed using Microreact⁴⁶ were analyzed with RELAX.⁴⁷ Comparison of the TrpA and TrpB trees provides insights about the evolution of these interacting enzymes (Figure 6a). The TrpA and TrpB enzymes show dissimilar evolutionary rates and better explain our structural and biochemical results. The regulatory and

physiological regimen of *C. trachomatis* (and *C. suis*) mediated by indole implies different selection pressures on these otherwise evolutionary balanced enzymes, each one adopting a novel role than that seen in standard L-Trp synthases. Here, TrpA has accumulated mutations that render this enzyme catalytically inactive, yet maintaining a role as an structural scaffold and allosteric activator of TrpB, making the latter more functionally active. Indeed, after mutational analysis at the nucleotide level, we found that TrpA enzymes from *C. trachomatis* and *C. suis* are under relaxation of purifying selection, at least partially (Table S4), when compared with their homologs from all other organisms analyzed with a complete TrpA enzyme complement (Figure 6b). This result contrasts with that seen for TrpB enzymes, which show an unequivocal signal of intensifying selection (Table S5). The general evolutionary trend depicted by this analysis can be corroborated by mutations revealed by the multiple sequence alignment obtained within this comparative evolutionary genomics framework (Figure S1, S2).

As previously reported, TrpA of *C. trachomatis* ocular strain A/Har-13 (and most of the ocular serovar strains A, Ba, C, Da) is truncated at its C terminal end in the α L6. Deletion of nt 528 resulted in the introduction of a stop codon at nt 550-552, rendering a polypeptide that may not fold into a functional, globular protein. This may be related to the sterile eye environment that explains the ocular tropism, where there is no associated microbiota that secretes indole for tryptophan synthesis.³⁷ Observations of TrpA phylogeny at the amino acid level (Table S6, Figure S1A) recapitulate the evolutionary relationship of seven *Chlamydia* ocular strains: Serovar Ba (strain AP2), Serovar Da (strain Da/TW-448), Serovar A (strain A/Har-13 [3]), Serovar C (strain C-TW-3 [2]), which group together in a sub-branch shown also in Figure 6a in the *C. trachomatis* clade. Interestingly, mutation of *St* β Pro270 to β Arg267 in the cation binding pocket conserved only in *Chlamydia* (Figure 2, S3, Table S7) predicts that the β reaction should be less sensitive to solution composition.

Taking into account results from relaxation of selection analyses and changes at position level in TrpA, it is plausible to propose that this subunit has a pivotal role for regulation of tryptophan synthase function. Changes in TrpA must correlate with adaptations of *Chlamydiae* species depending on the metabolic conditions in their microenvironment (tissue and organism where they reside). The results of the CORASON analysis confirms previous observations about gene content, with *C. trachomatis* and *C. suis* only having *trpA* and *trpB* genes, and the remaining organisms possessing complete *trpE(G)DCFBA* operons, other than *Chlamydiales bacterium*, *Parachlamydia* sp., *C. pecorum*, *C. caviae*, and *C. felis*, which lack the genes for

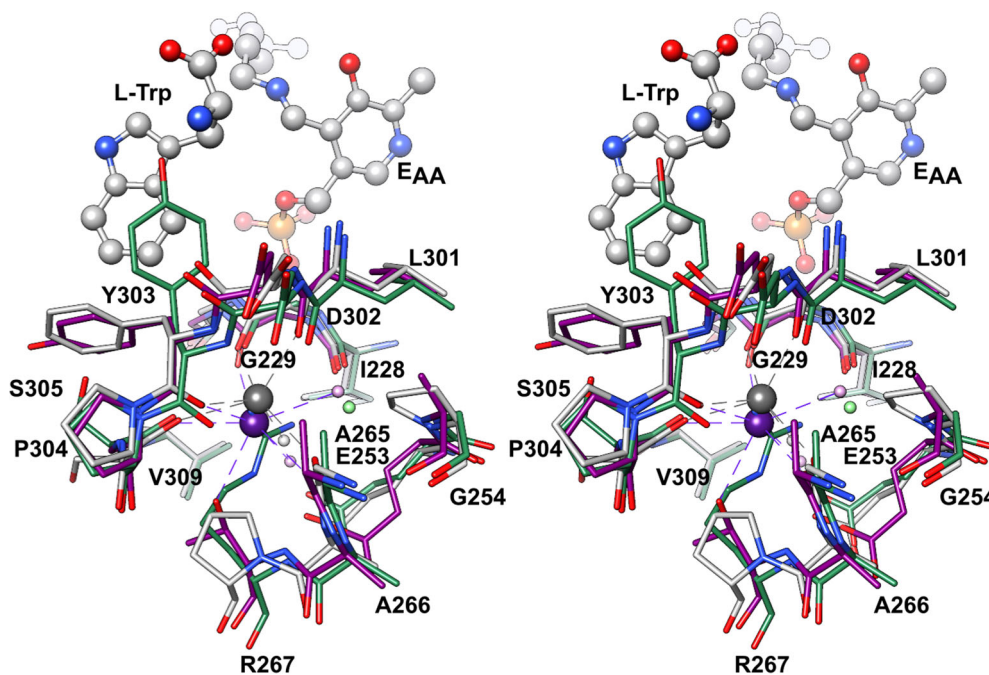


FIGURE 5 Monovalent cation-binding site. Stereoview of cation binding site superposition of *CtTrpB* (green) with *StTrpB* in complex with L-Trp (grey, chain B, Protein Data Bank [PDB] ID 5CGQ) and *MtTrpAB* (purple, chain D, PDB ID 5TCF). The L-Trp ligand and Lys-pyridoxal 5'-phosphate (PLP) adduct from the *StTrpAB* structure are shown in a ball-and-stick model. Cesium cations from the *StTrpAB* and *MtTrpAB* structures are shown as spheres, in grey and purple, respectively. The smaller spheres represent water molecules, color-coded as their respective proteins. Coordination sphere shown in dash lines

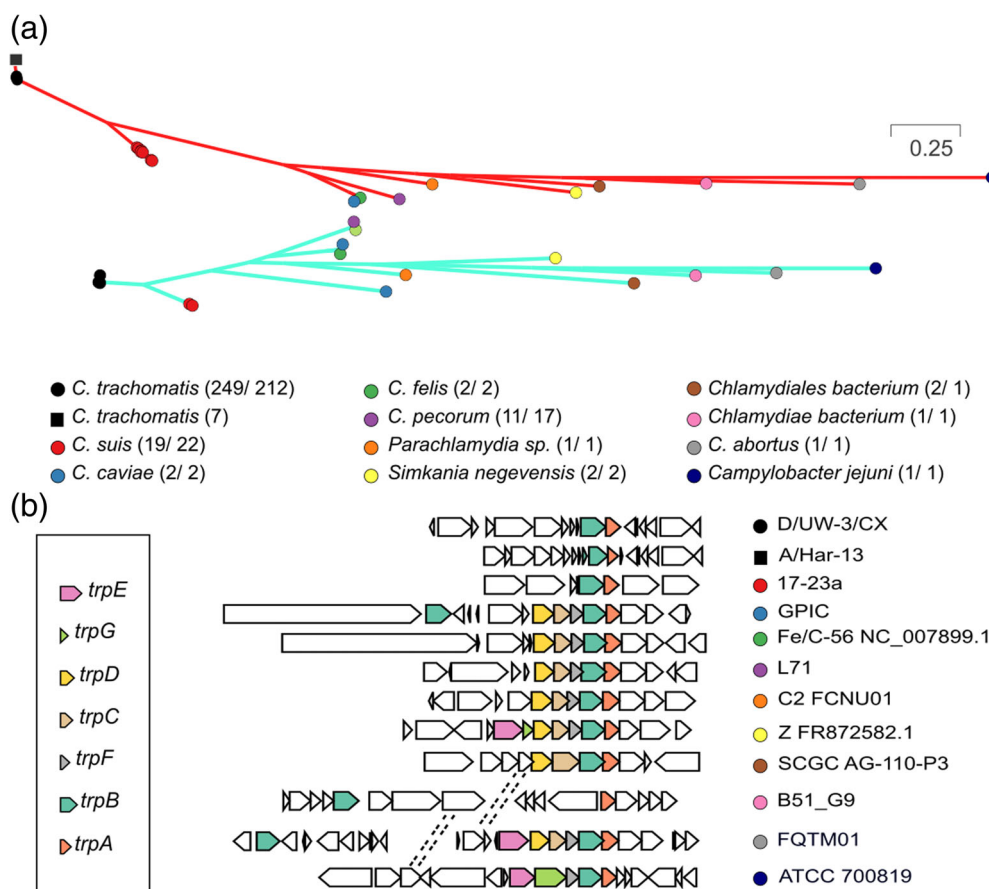


FIGURE 6 *Chlamydiae trpA* and *trpB* trees (a) and phylogenetic reconstruction and phylogenetic context analysis (b). Phylogeny construction of 294 *TrpA* (red) and 263 *TrpB* (cyan) amino acid sequences were performed as described in Materials and Methods Section 4. The number of sequences for *TrpA* and *TrpB* are shown in parenthesis. Different species are color-coded. Location and genetic context of *trpA* and *trpB* genes are shown in (b)

anthranilate synthase (Figure 6b). A complete *trp* operon is present in the outgroup provided by *Campylobacter jejuni*, but this seems to be deleted during the course of evolution in the abovementioned unclassified organism *C.*

bacterium B51_G9 and *C. abortus* FQTM01, which show duplicated *trpB* genes located at different positions in the chromosome, yet only a single copy of *trpA*. This similarity with bona fide *C. trachomatis* and *C. suis* isolates suggests

convergent evolution driven by similar metabolic constraints of their common tissue tropism. In contrast, *Chlamydiales bacterium* SCGC AG-110-P3 is more similar, with a complete *trp* operon, to non-human species, including isolates of *C. caviae*, *C. felis*, *C. pecorum* and *Parachlamydia* sp. Of these organisms, only *C. caviae* shows a difference in that it has two *trpB* copies in close proximity (Figure 6b).

2.7 | TrpA active site in *Chlamydia* species

In TrpA of *C. trachomatis* and *C. suis* several mutations accumulate in the active site. As discussed before, *C. trachomatis* preserves the catalytic residues, but at the same time residues with large side chains (Arg205, Asp207, Lys227) are introduced in positions of glycine in catalytically active TrpAs, reducing the pocket size, most likely preventing substrate binding. The positively charged side chain of Arg206, replacing large, hydrophobic phenylalanine needed for interaction with the indole ring, is another striking change. The same pattern is observed in *C. suis*, with the exception of the latter mutation introducing Lys, not Arg. These positions potentially discriminate between catalytically active and inactive TrpAs, with other members of the genus *Chlamydia* following the pattern seen in organisms with the complete tryptophan synthase enzymes complement, including functional TrpAB (Table S6, Figures S1A, S2).

Additional substitutions that influence the TrpA's pocket size in a less dramatic way, are Ile123 and Tyr95. First, Ile123 substitution is present in *C. trachomatis* and *C. suis*, which in most of the *Chlamydiae* species, including *C. caviae*, *C. felis*, *C. pecorum*, *Chlamydiales bacterium*, *Parachlamydia* sp., and the closely-related *Simkania negevensis*, this position is adopted by a smaller side-chain valine, while *C. abortus* and *Campylobacter jejuni* have proline. In the so-called *Chlamydiae bacterium*, a smaller side-chain residue (Val or Pro) is substituted by leucine instead of isoleucine. Second, Tyr95 substitution is present in *C. trachomatis* and *C. suis*, whereas TrpA homologs of all of *Chlamydiae* species have an analogous bulky side-chain phenylalanine, which is replaced by Met in *S. negevensis* and *Campylobacter jejuni*. As previously mentioned, the introduction of these large (Ile) and bulky (Tyr) side-chain residues where conserved smaller (Val, Pro, Ala, Met) residues are usually found, suggest a reduced flexibility during indole binding and a reduced cavity volume, and so they may be reflecting a gradual loss of TrpA substrate binding capability in *C. trachomatis* and *C. suis* (Table S6, Figure S1A).

Overall, these observations are congruent with the evolutionary process suggested for TrpA and TrpB supported by the functional and structural characterization provided herein.

3 | CONCLUSIONS

Chlamydia are obligate intracellular pathogens with a complex developmental cycle. In response to reduced metabolic capabilities under L-Trp starvation, *Chlamydia* retracts into the persistent aRB state, which has an alternative translation profile from other forms, as has been shown for genital *C. trachomatis* D/UW-3/CX.⁴⁸ The proteome features reflect the physiological needs of a given bacterial phenotype, for example, gene products necessary for rapid growth, such as those involved in cell envelope biosynthesis show high abundance in EBs and are much lower in RB and aRB. On the other hand, both RB and aRB show rapid translation, due to higher quantities of ribosomal proteins than observed in EB. The most striking feature of the aRB phenotype is a significant increase of TrpA and TrpB levels—from less than 0.05% in EB to 9% of total protein in aRB—making tryptophan synthase the second most abundant protein of the persistent state. Interestingly, proteins produced in aRB have lower L-Trp content while those made during RB proliferation, in the course of evolution, maximized their L-Trp content, making the EB to RB to aRB differentiation process strongly dependent on L-Trp availability.^{49,50} Strains with functional TrpAB may therefore have an advantage in the infectious process, provided that other necessary metabolites are available.

Access to L-Trp is required during infection and survival, yet the organism has lost most genes in L-Trp biosynthesis. The few remaining genes include *trpA* and *trpB* encoding two subunits of tryptophan synthase. To understand the role of chlamydial TrpAB at the molecular level, we have purified and characterized recombinant $\alpha\beta\beta\alpha$ tryptophan synthase from *C. trachomatis*. We show here that this enzyme has some unusual properties. Its α subunit has lost the ability to produce indole but at the same time it seems required for high activity of the β subunit, which uses indole, most likely produced by co-inhabiting bacteria, to make L-Trp. Our structural and biochemical data combined with genomic analysis explain the observed enzyme properties. The TrpA subunit preserves the key conserved catalytic residues but other active site mutations prevent it from binding the IGP substrate and so it cannot produce indole. At the same time, the TrpB subunit is fully functional and can use indole, L-Ser and the PLP cofactor to synthesize L-Trp. Though the β subunit is active in the absence of the α subunit, its activity is enhanced almost four times when in

complex with α , providing a significant metabolic advantage to the pathogen during certain steps of its developmental cycle. Therefore, although TrpA lost its catalytic activity it still maintains its allosteric function. We also suggest that the CtTrpAB activity is much less dependent on the presence of monovalent metal cations since mutation of Pro267 to arginine seems to provide a permanent side chain serving as a fixed cation effector. Our studies suggest that targeting CtTrpB for drug development may be an effective approach for control of *C. trachomatis* infections.

4 | METHODS

4.1 | Cloning *trpA* and *trpB* genes

The *trpB* gene was amplified from *C. trachomatis* D/UW-3/CX genomic DNA using the following primers: AGGAGGTTAGATATGTTCAAACATAAACATCCTTT-TGGGGGA and GTGATGGTGATGATGCTCATAAATT CCTCTGTTTCTGCGGATG. The PCR product was purified and treated with T4 polymerase in the presence of dCTP according to previously published methods⁵¹ followed by ligation-independent cloning to pMCSG91 (ampicillin resistance) to give Ct-*trpB*-pMCSG91. TrpB was expressed with C-terminal non-cleavable His₆-tag. Similarly, *trpA* gene was amplified with primers AGGAGGTTAGATATGAGTAAATTAACCCAAGTTTT-TAAACAATAAGCTAT and GTGATGGTGATGATG TTATCCAGGAATAACTGTTTGTGCAAGTGCA. The PCR product was purified, T4 polymerase treated and cloned into vector pMCSG89 that carries kanamycin resistance. TrpA was expressed without any tag, the expression plasmid was named Ct-*trpA*-pMCSG89. The *E. coli* BL21-Gold (DE3) cells were co-transformed with sequence-confirmed plasmids and selected against ampicillin (150 μ g/ml) and kanamycin (30 μ g/ml) in LB medium supplemented with 40 mM K₂HPO₄ and 2 g glucose per liter (LB-PO₄-glucose medium). A starter culture was grown overnight at 37°C on a shaker set to 200 rpm. The following morning, 12 L of LB-PO₄-glucose medium with antibiotics was inoculated with overnight culture. After reaching OD₆₀₀ of 1.0, the culture was cooled to 20°C and supplemented with 50 μ M PLP, and protein expression was induced with 0.3 mM IPTG. The growth was continued for another 20 hr at 20°C and at 190 rpm. An additional 6 L LB medium culture with only Ct-*trpA*-pMCSG89 were grown under the same conditions. Finally, cells were harvested and suspended in buffer A (50 mM HEPES:NaOH, pH 7.5; 150 mM KCl; 20 mM imidazole, pH 8.0; 5% glycerol; 1 mM TCEP; 1 mM PLP; 1 mM L-Ser). The cell suspension was frozen and stored at -80°C.

4.2 | TrpAB expression, purification and crystallization

Frozen cells were thawed and sonicated (5 min total time, 130 W power output) and spun at 30,000 \times g at 4°C for 1 hr. The initial Ni²⁺ affinity purification step was performed using a 2.5 cm \times 10 cm Flex-Column connected to a Van-Man vacuum manifold (Promega). Supernatant was loaded on 5 ml Ni²⁺ Sepharose (GE Healthcare Life Sciences) equilibrated with buffer A and mixed thoroughly with the resin. Vacuum of 15 psi was used to speed removal of supernatant as well as to wash out of unbound proteins (200 ml buffer A). The TrpAB complex was eluted with 25 ml buffer A supplemented with 500 mM imidazole, pH 8.0. The eluate was concentrated to about 2 ml and loaded on a Superdex 200 16/70 size exclusion column (GE Healthcare Life Sciences) equilibrated with buffer A. Successful crystallization required the presence of two protein peaks, one containing the TrpAB complex and another containing excess of the TrpA subunit. Fractions containing the TrpAB complex were collected, and buffer A was replaced with crystallization buffer (20 mM HEPES:NaOH, pH 8.0, 150 mM KCl; 1 mM PLP, 1 mM L-Ser, 1.5 mM TCEP) on Amicon 30 kDa cutoff concentrators (Millipore). The protein complex was concentrated to ~33.2 mg/ml.

Crystallization experiments were performed using the sitting-drop vapor-diffusion method in 96-well CrystalQuick plates (Greiner Bio-One, Monroe, NC) with the help of the Mosquito liquid dispenser (TTP LabTech, Cambridge, MA). Crystallizations trials were performed at 16°C using several protein-to-reservoir ratios (1:1; 1:3; 1:2 plus 4.7 mM L-serine) using Index and Peg/Ion (Hampton Research, Aliso Viejo, CA), MCSG1 (Anatrace Inc., Maumee, OH) and PEGsII (Qiagen Inc., Germantown, MD) screens. Immediately after preparation crystallization plates were wrapped in a foil to keep them in the dark. Small multiple crystals appeared in several conditions in 2–5 days. The best crystals of the TrpAB complex appeared at 16°C in the Index C11 condition (1.0 M Ammonium sulfate; 0.1 M HEPES pH 7.0; 0.5% wt/vol Polyethylene glycol 8,000). Further optimization with the additive screen from Hampton at 16°C and 2:1 protein-to-reservoir ratio produced robust diffraction-quality crystals with 1,5-diaminopentane.

4.3 | Data collection, structure solution and refinement

The crystal was washed in the crystallization solution supplemented with 28% sucrose for cryoprotection and flash-cooled in liquid nitrogen. The X-ray diffraction images were recorded on the Pilatus3 X 6 M detector at

TABLE 2 Data processing and refinement statistics

Data collection	
Wavelength (Å)	0.9792
Resolution range (Å) ^a	30.00–2.42 (2.46–2.42)
Space group	C222 ₁
Unit cell (Å)	$a = 114.92$ $b = 133.90$ $c = 128.43$
Unique reflections (merged)	37,871 (1,857)
Multiplicity	11.4 (6.2)
Completeness (%)	99.9 (99.9)
$\langle I \rangle / \langle \sigma I \rangle$	9.90 (1.55)
Wilson B-factor (Å ²)	26.0
R_{merge}^b	0.342 (1.356)
CC1/2 ^c	0.653
Refinement	
Resolution range (Å)	29.84–2.42
Reflections work/test	35,961/1,876
$R_{\text{work}}/R_{\text{free}}^d$	0.16/0.19
Number of non-hydrogen atoms	
Macromolecules	4,931
Ligands/solvent	56/222
RMSD (bonds) (Å)	0.007
RMSD (angles) (°)	0.931
Ramachandran favored ^e (%)	97.61
Ramachandran outliers (%)	0.16
Rotamer outliers (%)	1.91
Clashscore	4.02
Average B-factor (Å ²)	
Macromolecules	36.8
Ligands	50.9
Solvent	35.4
Number of TLS groups	10
PDB ID	6V82

Abbreviation: PDB, Protein Data Bank.

^aValues in parentheses correspond to the highest resolution shell.

^b $R_{\text{merge}} = \sum h \sum j |I_{hj} - \langle I_{hj} \rangle| / \sum h \sum j I_{hj}$, where I_{hj} is the intensity of observation j of reflection h .

^cLast shell, as defined by.⁶¹

^d $R = \sum h |F_o| - |F_c| / \sum h |F_o|$ for all reflections, where F_o and F_c are observed and calculated structure factors, respectively. R_{free} is calculated analogously for the test reflections, randomly selected and excluded from the refinement.

^eAs defined by Molprobit⁶² and implemented in Phenix.

the Structural Biology Center 19-ID beamline at the Advanced Photon Source, Argonne National Laboratory. The dataset was processed with the HKL3000 suite.⁵² Intensities were converted to structure factor amplitudes in the Ctruncate program^{53,54} from the CCP4 package.⁵⁵

The data collection and processing statistics are given in Table 2.

The structure was solved by molecular replacement in Phaser⁵⁶ with individual subunits of TrpAB from *F. tularensis* as search templates (PDB ID 5KZM). The initial model was built in Phenix⁵⁷ and Arp/wARP and subsequently improved by manual modifications in Coot⁵⁸ and crystallographic refinement in Phenix.⁵⁹ The refinement statistics are given in Table 2. The atomic coordinates and structure factors have been deposited in the PDB under accession code 6V82.

4.4 | Cα atoms superpositions

The superpositions have been carried out in Superpose program from the CCP4 suite⁵⁵ via secondary structure matching algorithm. The following structures were used in calculations: 5K9X, 5KZM, 5KIN, 1BKS, 5KMY, 6HUL, 5E0K, 5TCF.

4.5 | Measurement of enzyme kinetics in the β-elimination reaction

Activity in the β-elimination reaction was measured as previously reported.^{13,31} Briefly, TrpB or TrpAB (1 μM) was incubated at room temperature in 20 mM HEPES pH 8.0, 100 mM KCl, 0.5 mM TCEP, and 40 μM PLP (TrpAB buffer) with indole and L-Ser. k_{cat}^{β} was measured under saturating indole (200 μM) and L-Ser concentrations (20 mM) and K_M^{Ser} was measured under saturating indole and variable L-Ser concentrations. Absorbance of 290 nm light was measured using a SpectraMax M5 (Molecular Devices) and reaction progress curves were determined over a period in which product generation was linear. The difference in extinction coefficient between tryptophan and indole at 290 nm ($\Delta\epsilon = 1890 \text{ M}^{-1} \text{ cm}^{-1}$) was used to calculate the rate of the reaction.³⁹ Data reflect $n \geq 3$ independent experiments.

4.6 | Measurement of enzyme kinetics in the α reaction

Activity in the α reaction was measured using a coupled assay as previously reported.¹³ Briefly, IGP (500 μM), with or without L-Ser (20 mM), was diluted in TrpAB buffer with 50 μg/ml glyceraldehyde 3-phosphate dehydrogenase (GAPDH), 2.5 mM NAD⁺, and 0.015 M sodium pyrophosphate (pH 8.5) with 0.03 M sodium arsenate. TrpA or TrpAB (5 μM) was added to start the reaction and activity was monitored by the production of

NADH (excitation 340 nm, $\epsilon_{340} = 6,220 \text{ M}^{-1} \text{ cm}^{-1}$). Data reflect $n \geq 3$ independent experiments.

4.7 | Comparative genomics analysis

A total of 294 TrpA and 263 TrpB protein sequences from *Chlamydia* and closely related organisms were retrieved from NCBI repository database. Moreover, when available, genome sequences of these organisms were also obtained (262 in total). A set of related information including Accessions, IDs, organisms, strains, isolation tissue, location and year of isolation were manually collected from the gene data bank and from publications related to these sequences. Collected information was deposited as metadata's sequences files provided in supplementary files (Table S1, S2). Data from the genus *Simkania* was also included due to the similarity of their TrpA and TrpB sequences with *Chlamydia*-related isolates whose taxonomic identification remains uncertain (e.g., "*Chlamydiales bacterium* SCGC AG-110-P3" and "*Chlamydiae bacterium* B51_G9"). *Campylobacter* was used as an outgroup. Manual curation of genomic sequences allowed us to identify contaminated sequences, which were removed from our analysis as they provided divergent *C. trachomatis* TrpA sequences that confounded our analyses (Table S1, S2, S3). For the phylogenetic reconstructions, amino acid sequences were aligned with clustalo: v1.2.4-2-deb_cv1 docker biocontainer. The output files were used to align by codon the nucleotide sequences with RevTrans v1.4 web server. Stop codons were removed where needed. In the resultant nucleotide alignments, nucleotides were shaved in regions where more than 50% of occupancy was represented by gaps. Trees were constructed by using PHYML GTR model with default parameters in Seaview. Trees were rooted with *Campylobacter jejuni* as outgroup (Figure 6a). Interactive visualization of the trees are available in Microreact.⁴⁶ The TrpA tree can be found at <https://microreact.org/project/sHa1iaiPdHEU8gq57Y3kh6/a071bb07>, and TrpB tree at <https://microreact.org/project/5hnNa8e99xoasbeCTjyMSi/f238f3ee>. Tree and metadata files are available for download.

RELAX is specialized in detection of relaxation or intensification of natural selection in a specified set of branches.⁴⁷ Selection analysis within the *trpA* and *trpB* phylogenetic trees was done by defining *C. trachomatis* and/or *C. suis* as "test" branches and *C. pecorum* and/or all other branches as "reference" branches. Branches were labeled in the trees using the phylotree web server. A p value $\leq .05$ was set as threshold to take an intensification/relaxation selection result as significant. Results are

resumed and listed in Tables S4 and S5. Genome context was analyzed with CORASON with *trpA* and *trpB* gene sequences used as queries.⁴⁵ CORASON found both sequences in the interrogated *Chlamydiae* genomes and retrieved them with gene vicinities located at 10 kb upstream and downstream. Colors for each *trp* related gene added manually (Figure 6b). All comparative genomics analysis data are within the manuscript and its Supporting Information files.

ACKNOWLEDGMENTS

We thank Paula Bulaon for proof reading this manuscript. Funding for this project was provided by federal funds from the National Institute of Allergy and Infectious Diseases, National Institutes of Health, Department of Health and Human Services, under Contracts No. HHSN272201200026C and HHSN272201700060C (Andrzej Joachimiak). The use of SBC beamlines at the Advanced Photon Source is supported by the U.S. Department of Energy (DOE) Office of Science and operated for the DOE Office of Science by Argonne National Laboratory under Contract No. DE-AC02-06CH11357 (Andrzej Joachimiak). This research was also funded by a Newton Advanced Fellowship of the Royal Society, UK (NAF\R2\180631) (Francisco Barona-Gómez) and Conacyt, Mexico (CB-2016-01 No. 285746) (Francisco Barona-Gómez).

CONFLICT OF INTEREST

The authors declare that they have no conflicts of interest with the contents of this article. The content is solely the responsibility of the authors and does not necessarily represent the official views of the National Institutes of Health.

AUTHOR CONTRIBUTIONS

Karolina Michalska: Conceptualization; investigation; visualization; writing-original draft; writing-review & editing. **Samantha Wellington:** Investigation; methodology; writing-original draft. **Natalia Maltseva:** Investigation; methodology. **Robert Jędrzejczak:** Investigation; methodology. **Nelly Selem-Mojica:** Data curation; investigation; methodology; visualization; writing-original draft. **Rodrigo Rosas-Becerra:** Investigation; visualization; writing-original draft. **Francisco Barona-Gomez:** Data curation; funding acquisition; methodology; project administration; supervision; writing-original draft. **Deborah Hung:** Funding acquisition; project administration; supervision. **Andrzej Joachimiak:** Conceptualization; funding acquisition; project administration; supervision; writing-original draft; writing-review & editing.

ORCID

Francisco Barona-Gómez  <https://orcid.org/0000-0003-1492-9497>

Andrzej Joachimiak  <https://orcid.org/0000-0003-2535-6209>

REFERENCES

- WHO guidelines for the treatment of *Chlamydia trachomatis*. Geneva, 2016. World Health Organization.
- Jones RB, Van der Pol B, Martin DH, Shepard MK. Partial characterization of chlamydia trachomatis isolates resistant to multiple antibiotics. *J Infect Dis*. 1990;162:1309–1315.
- Somani J, Bhullar VB, Workowski KA, Farshy CE, Black CM. Multiple drug-resistant chlamydia trachomatis associated with clinical treatment failure. *J Infect Dis*. 2000;181:1421–1427.
- Sandoz KM, Rockey DD. Antibiotic resistance in Chlamydiae. *Future Microbiol*. 2010;5:1427–1442.
- Grayston JT, Aldous MB, Easton A, et al. Evidence that chlamydia pneumoniae causes pneumonia and bronchitis. *J Infect Dis*. 1993;168:1231–1235.
- Di Pietro M, Filardo S, Romano S, Sessa R. Chlamydia trachomatis and chlamydia pneumoniae interaction with the host: Latest advances and future prospective. *Microorganisms*. 2019;7:140.
- Bodetti TJ, Jacobson E, Wan C, et al. Molecular evidence to support the expansion of the hostrange of Chlamydomydia pneumoniae to include reptiles as well as humans, horses, koalas and amphibians. *Syst Appl Microbiol*. 2002;25:146–152.
- Cheong HC, Lee CYQ, Cheok YY, Tan GMY, Looi CY, Wong WF. Chlamydiae: Diseases in primary hosts and zoonosis. *Microorganisms*. 2019;7:146.
- Abdelrahman YM, Belland RJ. The chlamydial developmental cycle. *FEMS Microbiol Rev*. 2005;29:949–959.
- Hogan RJ, Mathews SA, Mukhopadhyay S, Summersgill JT, Timms P. Chlamydial persistence: Beyond the biphasic paradigm. *Infect Immun*. 2004;72:1843–1855.
- Akashi H, Gojobori T. Metabolic efficiency and amino acid composition in the proteomes of Escherichia coli and Bacillus subtilis. *Proc Natl Acad Sci U S A*. 2002;99:3695–3700.
- Zhang YJ, Reddy MC, Ioerger TR, et al. Tryptophan biosynthesis protects mycobacteria from CD4 T-cell-mediated killing. *Cell*. 2013;155:1296–1308.
- Wellington S, Nag PP, Michalska K, et al. A small-molecule allosteric inhibitor of *Mycobacterium tuberculosis* tryptophan synthase. *Nat Chem Biol*. 2017;13:943–950.
- Peng K, Monack DM. Indoleamine 2,3-dioxygenase 1 is a lung-specific innate immune defense mechanism that inhibits growth of Francisella tularensis tryptophan auxotrophs. *Infect Immun*. 2010;78:2723–2733.
- Rhee S, Parris KD, Ahmed SA, Miles EW, Davies DR. Exchange of K⁺ or Cs⁺ for Na⁺ induces local and long-range changes in the three-dimensional structure of the tryptophan synthase alpha2beta2 complex. *Biochemistry*. 1996;35:4211–4221.
- Rhee S, Parris KD, Hyde CC, Ahmed SA, Miles EW, Davies DR. Crystal structures of a mutant (betaK87T) tryptophan synthase alpha2beta2 complex with ligands bound to the active sites of the alpha- and beta-subunits reveal ligand-induced conformational changes. *Biochemistry*. 1997;36:7664–7680.
- Rhee S, Miles EW, Davies DR. Cryo-crystallography of a true substrate, indole-3-glycerol phosphate, bound to a mutant (alphaD60N) tryptophan synthase alpha2beta2 complex reveals the correct orientation of active site alphaGlu49. *J Biol Chem*. 1998;273:8553–8555.
- Schneider TR, Gerhardt E, Lee M, Liang PH, Anderson KS, Schlichting I. Loop closure and intersubunit communication in tryptophan synthase. *Biochemistry*. 1998;37:5394–5406.
- Sachpatzidis A, Dealwis C, Lubetsky JB, Liang PH, Anderson KS, Lolis E. Crystallographic studies of phosphonate-based alpha-reaction transition-state analogues complexed to tryptophan synthase. *Biochemistry*. 1999;38:12665–12674.
- Weyand M, Schlichting I. Crystal structure of wild-type tryptophan synthase complexed with the natural substrate indole-3-glycerol phosphate. *Biochemistry*. 1999;38:16469–16480.
- Weyand M, Schlichting I. Structural basis for the impaired channeling and allosteric inter-subunit communication in the beta A169L/beta C170W mutant of tryptophan synthase. *J Biol Chem*. 2000;275:41058–41063.
- Kulik V, Weyand M, Seidel R, et al. On the role of alphaThr183 in the allosteric regulation and catalytic mechanism of tryptophan synthase. *J Mol Biol*. 2002;324:677–690.
- Weyand M, Schlichting I, Herde P, Marabotti A, Mozzarelli A. Crystal structure of the beta Ser178-> pro mutant of tryptophan synthase. A "knock-out" allosteric enzyme. *J Biol Chem*. 2002;277:10653–10660.
- Weyand M, Schlichting I, Marabotti A, Mozzarelli A. Crystal structures of a new class of allosteric effectors complexed to tryptophan synthase. *J Biol Chem*. 2002;277:10647–10652.
- Kulik V, Hartmann E, Weyand M, et al. On the structural basis of the catalytic mechanism and the regulation of the alpha subunit of tryptophan synthase from salmonella typhimurium and BX1 from maize, two evolutionarily related enzymes. *J Mol Biol*. 2005;352:608–620.
- Blumenstein L, Domratcheva T, Niks D, et al. BetaQ114N and betaT110V mutations reveal a critically important role of the substrate alpha-carboxylate site in the reaction specificity of tryptophan synthase. *Biochemistry*. 2007;46:14100–14116.
- Ngo H, Kimmich N, Harris R, et al. Allosteric regulation of substrate channeling in tryptophan synthase: Modulation of the L-serine reaction in stage I of the beta-reaction by alpha-site ligands. *Biochemistry*. 2007;46:7740–7753.
- Lai J, Niks D, Wang Y, et al. X-ray and NMR crystallography in an enzyme active site: The indoline quinonoid intermediate in tryptophan synthase. *J Am Chem Soc*. 2011;133:4–7.
- Niks D, Hilario E, Dierkers A, et al. Allostery and substrate channeling in the tryptophan synthase holoenzyme complex: Evidence for two subunit conformations and four quaternary states. *Biochemistry*. 2013;52:6396–6411.
- Hilario E, Caulkins BG, Huang YM, et al. Visualizing the tunnel in tryptophan synthase with crystallography: Insights into a selective filter for accommodating indole and rejecting water. *Biochim Biophys Acta*. 1864;2016:268–279.
- Michalska K, Gale J, Joachimiak G, et al. Conservation of the structure and function of bacterial tryptophan synthases. *IUCrJ*. 2019;6:649–664.
- Lee SJ, Ogasahara K, Ma J, et al. Conformational changes in the tryptophan synthase from a hyperthermophile upon alpha2beta2 complex formation: Crystal structure of the complex. *Biochemistry*. 2005;44:11417–11427.

33. Buller AR, Brinkmann-Chen S, Romney DK, Herger M, Murciano-Calles J, Arnold FH. Directed evolution of the tryptophan synthase beta-subunit for stand-alone function recapitulates allosteric activation. *Proc Natl Acad Sci U S A*. 2015;112:14599–14604.
34. Jeong MS, Jeong JK, Lim WK, Jang SB. Structures of wild-type and P28L/Y173F tryptophan synthase alpha-subunits from *Escherichia coli*. *Biochem Biophys Res Commun*. 2004;323:1257–1264.
35. Nishio K, Morimoto Y, Ishizuka M, Ogasahara K, Tsukihara T, Yutani K. Conformational changes in the alpha-subunit coupled to binding of the beta 2-subunit of tryptophan synthase from *Escherichia coli*: Crystal structure of the tryptophan synthase alpha-subunit alone. *Biochemistry*. 2005;44:1184–1192.
36. Dunn MF. Allosteric regulation of substrate channeling and catalysis in the tryptophan synthase holoenzyme complex. *Arch Biochem Biophys*. 2012;519:154–166.
37. Fehlner-Gardiner C, Roshick C, Carlson JH, et al. Molecular basis defining human chlamydia trachomatis tissue tropism. A possible role for tryptophan synthase. *J Biol Chem*. 2002;277:26893–26903.
38. Caldwell HD, Wood H, Crane D, et al. Polymorphisms in chlamydia trachomatis tryptophan synthase genes differentiate between genital and ocular isolates. *J Clin Invest*. 2003;111:1757–1769.
39. Lane AN, Kirschner K. The catalytic mechanism of tryptophan synthase from *Escherichia coli*. Kinetics of the reaction of indole with the enzyme-L-serine complexes. *Eur J Biochem*. 1983;129:571–582.
40. Yang XJ, Miles EW. Threonine 183 and adjacent flexible loop residues in the tryptophan synthase alpha subunit have critical roles in modulating the enzymatic activities of the beta subunit in the alpha 2 beta 2 complex. *J Biol Chem*. 1992;267:7520–7528.
41. Fan YX, McPhie P, Miles EW. Regulation of tryptophan synthase by temperature, monovalent cations, and an allosteric ligand. Evidence from Arrhenius plots, absorption spectra, and primary kinetic isotope effects. *Biochemistry*. 2000;39:4692–4703.
42. Lane AN, Kirschner K. Mechanism of the physiological reaction catalyzed by tryptophan synthase from *Escherichia coli*. *Biochemistry*. 1991;30:479–484.
43. Peracchi A, Mozzarelli A, Rossi GL. Monovalent cations affect dynamic and functional properties of the tryptophan synthase alpha 2 beta 2 complex. *Biochemistry*. 1995;34:9459–9465.
44. Fan YX, McPhie P, Miles EW. Guanidine hydrochloride exerts dual effects on the tryptophan synthase alpha 2 beta 2 complex as a cation activator and as a modulator of the active site conformation. *Biochemistry*. 1999;38:7881–7890.
45. Navarro-Munoz JC, Selem-Mojica N, Mullowney MW, et al. A computational framework to explore large-scale biosynthetic diversity. *Nat Chem Biol*. 2020;16:60–68.
46. Argimon S, Abudahab K, Goater RJE, et al. Microreact: Visualizing and sharing data for genomic epidemiology and phylogeography. *Microb Genom*. 2016;2:e000093.
47. Wertheim JO, Murrell B, Smith MD, Kosakovsky P, Scheffler K. RELAX: Detecting relaxed selection in a phylogenetic framework. *Mol Biol Evol*. 2015;32:820–832.
48. Ostergaard O, Follmann F, Olsen AW, Heegaard NH, Andersen P, Rosenkrands I. Quantitative proteomic profiling of chlamydia trachomatis growth forms reveals defense strategies against tryptophan starvation. *Mol Cell Proteomics*. 2016;15:3540–3550.
49. Lo CC, Xie G, Bonner CA, Jensen RA. The alternative translational profile that underlies the immune-evasive state of persistence in Chlamydiae exploits differential tryptophan contents of the protein repertoire. *Microbiol Mol Biol Rev*. 2012;76:405–443.
50. Bonner CA, Byrne GI, Jensen RA. Chlamydia exploit the mammalian tryptophan-depletion defense strategy as a counter-defensive cue to trigger a survival state of persistence. *Front Cell Infect Microbiol*. 2014;4:17.
51. Kim Y, Babnigg G, Jedrzejczak R, et al. High-throughput protein purification and quality assessment for crystallization. *Methods*. 2011;55:12–28.
52. Minor W, Cymborowski M, Otwinowski Z, Chruszcz M. HKL-3000: The integration of data reduction and structure solution from diffraction images to an initial model in minutes. *Acta Cryst D*. 2006;62:859–866.
53. French S, Wilson K. Treatment of negative intensity observations. *Acta Cryst A*. 1978;34:517–525.
54. Padilla JE, Yeates TO. A statistic for local intensity differences: Robustness to anisotropy and pseudo-centering and utility for detecting twinning. *Acta Cryst D*. 2003;59:1124–1130.
55. Winn MD, Ballard CC, Cowtan KD, et al. Overview of the CCP4 suite and current developments. *Acta Cryst D*. 2011;67:235–242.
56. McCoy AJ. Solving structures of protein complexes by molecular replacement with Phaser. *Acta Cryst D*. 2007;63:32–41.
57. Adams PD, Baker D, Brunger AT, et al. Advances, interactions, and future developments in the CNS, Phenix, and Rosetta structural biology software systems. *Annu Rev Biophys*. 2013;42:265–287.
58. Emsley P, Cowtan K. Coot: Model-building tools for molecular graphics. *Acta Cryst D*. 2004;60:2126–2132.
59. Afonine PV, Grosse-Kunstleve RW, Echols N, et al. Towards automated crystallographic structure refinement with phenix.refine. *Acta Cryst D*. 2012;68:352–367.
60. Ahmed SA, Hyde CC, Thomas G, Miles EW. Microcrystals of tryptophan synthase alpha 2 beta 2 complex from salmonella typhimurium are catalytically active. *Biochemistry*. 1987;26:5492–5498.
61. Karplus PA, Diederichs K. Linking crystallographic model and data quality. *Science*. 2012;336:1030–1033.
62. Davis IW, Murray LW, Richardson JS, Richardson DC. MOLPROBITY: Structure validation and all-atom contact analysis for nucleic acids and their complexes. *Nucleic Acids Res*. 2004;32:W615–W619.

SUPPORTING INFORMATION

Additional supporting information may be found online in the Supporting Information section at the end of this article.

How to cite this article: Michalska K, Wellington S, Maltseva N, et al. Catalytically impaired TrpA subunit of tryptophan synthase from *Chlamydia trachomatis* is an allosteric regulator of TrpB. *Protein Science*. 2021;30:1904–1918. <https://doi.org/10.1002/pro.4143>